Liquid Nicotine Tamed in Solid Forms by Cocrystallization

CRYSTAL GROWTH & DESIGN

Article

pubs.acs.org/crystal

Liquid Nicotine Tamed in Solid Forms by Cocrystallization

Davide Capucci,[†] Davide Balestri,[†] Paolo P. Mazzeo,[†,§] Paolo Pelagatti,[†] Katia Rubini,[‡] and Alessia Bacchi*[,†,§]

[†]Dipartimento di Scienze Chimiche, della Vita e della Sostenibilità Ambientale, Università di Parma, Parco delle Scienze 17A, I-43124 Parma, Italy

[‡]Dipartimento di Chimica 'G. Ciamician', Università di Bologna, Via Selmi, 2, I-40126 Bologna, Italy

[§]Biopharmanet-tec, Parco delle Scienze, 27/A, I-43124 Parma, Italy

S *Supporting Information*

ABSTRACT: We address the problem of stabilizing liquid nicotine in solid forms at ambient conditions by cocrystallization. An intriguing aspect of nicotine lies in the fact that its crystal structure has never been reported in the literature, and this peculiarity may be ascribed to the liquid−glass transition that occurs when nicotine is supercooled under its melting point (−79 °C). Even though nicotine was considered a rigid molecule, its glass forming nature could be due to a certain extent of conformational variability, which has been assessed by a conformer search of the Cambridge Crystallographic Data Centre software. The design of cocrystals forms of nicotine is approached by analyzing its molecular electrostatic potential. On the basis of these considerations, three coformers have been identified, and their crystal structure shows that nicotine adapts to the packing features dictated by the coformers. The tool of packing energy frameworks has been used to discuss the stabilization of the cocrystals.

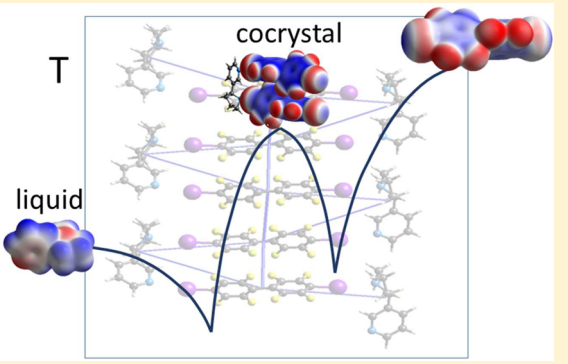

INTRODUCTION

Surprisingly, despite its fairly complex molecular structure, nicotine is a liquid. We address the problem of taming liquid nicotine in crystalline forms at ambient conditions. Crystallization at a given temperature is the result of a struggle between the destabilizing entropy contribution of the liquid state and the stabilizing enthalpy optimization by crystal ordering. Here we force the enthalpic stabilization by designing cocrystals of nicotine. The reason for this work stems from the fact that liquid formulations tend to be essentially less stable than solid forms; therefore most active pharmaceutical ingredients (APIs) and nutraceutical compounds are manufactured and distributed as crystalline materials,[1] and their action involves the delivery of the active molecule by a solubilization process either in the body or on the environment. However, some important molecules for human health are liquid at room temperature, and we are currently exploring general strategies to embed liquid ingredients in crystalline materials. Stabilization of liquid APIs is of enormous interest for pharmaceutical industries especially for storage, transportation, and handling. Liquid nicotine is a toxic alkaloid found in the leaves of the tobacco plants *Nicotiana tabacum* and *Nicotiana rustica* of the family *Solanaceae*[2]. Nicotine is also a nootropic stimulant drug. Because of its properties, nicotine has been of commercial interest and employed for widely different uses such as therapeutic use in treating nicotine dependence or as an insecticide.[3] Nicotine possesses two basic centers (Scheme 1); therefore salt formation could be exploited as a well-known method to build a crystalline material from a base; however, salification alters the molecular electronic and hydrogen bonding properties, as shown by computational simulation[4] and affords a material sensitive to pH. On the other hand, cocrystallization is considered a smart and dainty way to tune solubility properties of solid phases leaving the molecule chemically unchanged.[5] Despite this extremely high interest toward cocrystallization, no particular emphasis has been paid so far toward using it as a general means to stabilize liquid compounds: among the few reports stressing how to stabilize

Scheme 1. Nicotine and the Coformers Used in This Work

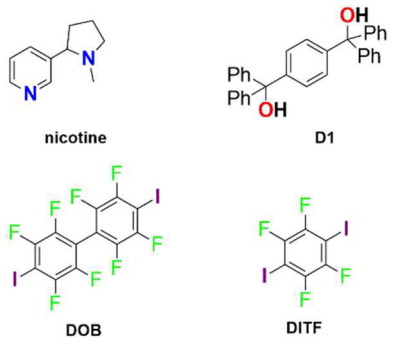

Received: June 23, 2017
Revised: August 3, 2017
Published: August 10, 2017

DOI: 10.1021/acs.cgd.7b00887
Cryst. Growth Des. XXXX, XXX, XXX−XXX

liquid APIs, we recently presented an investigation on the stability and solubility of cocrystals containing propofol, a widely used liquid anesthetic.[6] Cocrystallization of volatile or low melting compounds is an intriguing challenge, above all if the molecule of interest is of pharmaceutical or environmental relevance, or for the storage of gaseous compounds such as acetylene.[6−10] Aakeröy et. al have reported the stabilization of volatile iodoperfluoroalkanes, that are generally recognized as persistent potential pollutants, or even explosives, through cocrystallization in recent works.[11,12] On the other hand, only one cocrystal of neutral nicotine[13] has been reported in the literature, but no real stress has ever been given to the importance of stabilizing that compound through this methodology (a second example of highly disordered nicotine included in a crystalline sponge has been recently reported[14]).

An intriguing aspect of nicotine lies in the fact that its crystal structure as a pure compound has never been reported in the literature, and this peculiarity may be ascribed to the liquid−glass transition that occurs when nicotine is supercooled under its melting point (−79 °C).[15] Here we analyze the molecular features which make nicotine reluctant to form a solid and identify possible coformers to achieve cocrystallization (Scheme 1).

EXPERIMENTAL SECTION

Synthesis. (−)-Nicotine (99%), 1,4-diiodotetrafluorobenzene (98%), and all the solvents for crystallization were purchased from Sigma-Aldrich and used with no further purification in all crystallization experiments. 4,4′-Diiodooctafluorobiphenyl (DOB) has been synthesized starting from the commercial precursor 4,4′-dibromooctafluorobiphenyl (98%) from Sigma-Aldrich Chemical Co., following a literature reported procedure slightly modified (Supporting Information).[16,17] 1,4-Bis(diphenylhydroxymethyl)benzene (D1) has been synthesized from commercial precursor dimethyl terephthalate (99%, Sigma-Aldrich), following a literature reported procedure slightly modified[18] (see Supporting Information).

Cocrystallization. Cocrystallizations of (−)-nicotine and related coformers (di-iodotetrafluoro benzene (DITF), DOB, and D1) were carried out in ethyl acetate, tetrahydrofuran, and methanol. Solutions containing (−)-nicotine and the proper coformer with 1:1, 1:2, 2:1 molar ratios were left to slowly evaporate at room temperature until tiny single crystals suitable for single-crystal X-ray diffraction (SC-XRD) analysis formed. In all cases 1:1 cocrystals were obtained.

Thermal Analysis. Differential scanning calorimetry analysis on nicotine−DITF and nicotine−DOB cocrystals powder samples were performed with a PerkinElmer Diamond equipped with a model ULSP 90 ultracooler. Heating was carried out in open Al-pans at 5 °C/min in the temperature range from −25 to 80 °C. The enthalpy of the endothermic or exothermic event is determined by the integration of the area under the differential scanning calorimetry (DSC) peak, which is reported in J/g.

DSC trace of nicotine−D1 was collected with a PerkinElmer DSC 6000 in a sealed 50 μL Al-pan. The measurement was performed at atmospheric pressure under a constant flow of nitrogen (20 mL min^{-1}) in the temperature range from −30 to 110 °C. The enthalpy of the endothermic or exothermic event is determined by the integration of the area under the DSC peak, which is reported in J/g.

SC-XRD Analysis on Cocrystals. SC-XRD analysis was performed on single crystal samples at room temperature (293 K) on a SMART APEX2 diffractometer using Mo Kα radiation (λ = 0.71073 Å) for nicotine−DITF; Lorentz polarization and absorption correction were applied. Nicotine-DOB and nicotine-D1 were collected at 100 K under nitrogen flux at Elettra Sincrotrone (Trieste, Italy) at the XRD1 beamline with X-ray synchrotron radiation source and a NdBFe Multipole Wiggler (Hybrid linear) insertion device. Beam energy was set at 4.27 keV with a power of 8.6 kW and a beamsize fwhm of 2.0 × 0.37 mm (0.7 × 0.2 mm fwhm beam size on the sample) with photon flux 1012−1013 ph/sec. Pilatus 2 M detector was used to collect the data; synchrothron data were processed by using XDS software.[19] Structures were solved by direct methods using SHELXS[20] and refined by full-matrix least-squares on all F2 using SHELXL implemented in Olex2.[21] For nicotine−D1 and nicotine-DITF anisotropic displacement parameters were refined except for hydrogen atoms, while the crystal quality for nicotine−DOB allowed refinement of anisotropic thermal ellipsoids only for iodine atoms. Table 1 reports the results of crystal structures determination. CSD-Enterprise was used for crystal packing and conformational analysis within the CSD-Materials module.[22] Estimation of the interaction energy and energy frameworks were performed with CrystalExplorer17 using HF/3-21G basis set.[23,24] Molecular electrostatic potential (MEP) has been calculated with Tonto[25] using density functional theory (B3LYP) using the 6-311G(d,p) basis set and displayed using CrystalExplorer 17; MEP has been mapped on the electron density surface cut at the 0.002 e/$Å^3$ level. Crystallographic data for nicotine−D1, nicotine−DITF, and nicotine−DOB have been deposited with the Cambridge Crystallographic Data Centre as supplementary publication CCDC 1557603−1557605.

Table 1. Crystal Data and Structural Refinement

	nicotine−D1	nicotine−DITF	nicotine−DOB
empirical formula	$C_{42}H_{40}N_2O_2$	$C_{16}H_{14}F_4I_2N_2$	$C_{22}H_{14}F_8I_2N_2$
formula weight	604.76	564.09	712.15
temperature/K	100.15	293	100
crystal system	triclinic	monoclinic	monoclinic
space group	$P1$	$P2_1$	$P2_1$
a/Å	8.226(2)	10.65(2)	8.779(2)
b/Å	8.962(2)	12.12(2)	28.979(6)
c/Å	11.968(2)	14.71(3)	18.082(4)
α/°	86.84(3)	90	90
β/°	87.90(3)	91.35(3)	90.68(3)
γ/°	68.29(3)	90	90
volume/$Å^3$	818.3(3)	1898(6)	4600(2)
Z	1	4	8
ρ_{calc}, g/cm^3	1.227	1.974	2.057
μ/mm^{-1}	0.073	3.350	2.712
$F(000)$	322.0	1064.0	2704.0
radiation/Å	synchrotron (λ = 0.700)	MoKα (λ = 0.71073)	synchrotron (λ = 0.700)
2Θ range for data collection/°	3.358−65.624	2.77−47.076	2.614−40.932
reflections collected	15436	12857	13463
independent reflections	9058 [R_{int} = 0.0301, R_{sigma} = 0.0487]	5436 [R_{int} = 0.0985, R_{sigma} = 0.1363]	8799 [R_{int} = 0.1682, R_{sigma} = 0.2830]
data/restraints/parameters	9058/3/419	5436/7/387	8799/244/443
goodness-of-fit on F^2	1.066	0.955	1.053
final R indexes [$I \geq 2\sigma(I)$]	R_1 = 0.0408, wR_2 = 0.1035	R_1 = 0.0628, wR_2 = 0.1249	R_1 = 0.1374, wR_2 = 0.3413
final R indexes [all data]	R_1 = 0.0409, wR_2 = 0.1037	R_1 = 0.1473, wR_2 = 0.1588	R_1 = 0.2140, wR_2 = 0.3907
final ΔF max/min/e $Å^{-3}$	0.37/-0.32	1.02/-0.67	2.87/-1.92
Flack parameter	0.0(2)	0.06(6)	0.00(13)

RESULTS

In order to achieve cocrystallization, molecules with different functionalities are usually brought together relying on a wide toolkit of intermolecular interactions spanning from weak dispersive interactions to rather strong hydrogen or halogen

DOI: 10.1021/acs.cgd.7b00887
Cryst. Growth Des. XXXX, XXX, XXX−XXX

bonds. The predominant effect for molecular recognition is based on electrostatic complementarity.[26,27] A guidance to understand the propensity of a molecule to establish favorable intermolecular contacts through its functional groups is given by the MEP, calculated from the electron charge distribution, visualized on the molecular surface.[28,29] Figure 1 shows the

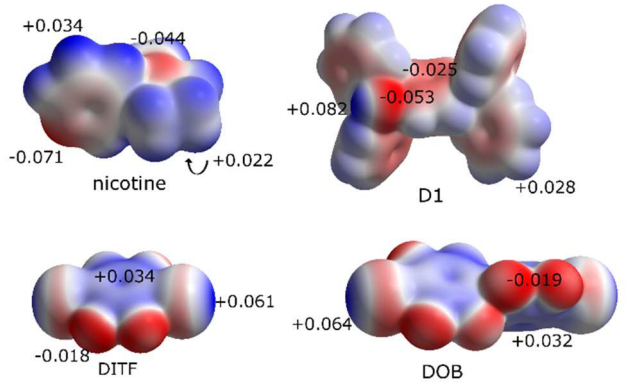

Figure 1. Molecular electrostatic potential (MEP) plotted on the electron density surface (drawn at the 0.002 au level) for nicotine, D1, DITF, and DOB. Significant local maximum and minimum values are reported (a.u.). The arrow indicates the charge on the pyrrolidine hidden surface.

electrostatic potential mapped on the molecular surface for nicotine, evidencing two remarkable negative spots corresponding to the nitrogen atoms, and a positive region at the pyrrolidine ring surface (hidden in Figure 1, view of the pyrrolidine ring is in the Supporting Information) and at the pyridine edge. The choice of coformers for nicotine was focused to small organic molecules able to interact with the negative spots of the nicotine MEP through suitable functional groups (Figure 1 and Scheme 1). Promising synthons have been selected considering both hydrogen bond and halogen bond interactions. Although early spectroscopic and computational works indicated the pyridinic nitrogen has much better hydrogen bond accepting capability,[30] it has been recently shown that both nitrogens can accept hydrogen bonds from water, with the pyridinic one being more efficient.[4] The same trend is here observed by comparing the MEP values corresponding to the two nitrogens (Figure 1). Previous works reported in the literature showed that 4,4′-bis-(diphenylhydroxymethyl)biphenyl is a wheel and axle molecule which efficiently enclathrated guest molecules among which nicotine.[13] Therefore we synthesized D1 as a potential good coformer for nicotine cocrystals. Diiodoperfluorurate aromatic derivatives have been described as efficient halogen bond donors (electron acceptors), which could equally well combine with the electron donor propensity of the nicotine nitrogens.[31] DITF and DOB have been chosen as halogen bonding coformers.

Crystal Structures. ORTEP drawings of all the structures are reported in the Supporting Information. Table 2 reports the significant supramolecular interactions.

Nicotine−D1 crystallizes in the chiral space group *P*1 in a 1:1 stoichiometric ratio. The molecular conformation of nicotine is determined by the torsion angle τ[C38−C34−C33−N1] = 140°, ruling the reciprocal orientation of the two nitrogen atoms (Figure 2). As expected from the design of the cocrystal, the crystal packing is dominated by the hydrogen bonds

Table 2. Hydrogen Bond and Halogen Bond Geometries

compound	pyridine N	pyrrolidine N
nicotine−D1	O···N = 2.790(2) Å	O···N (x, y + 1, z + 1) = 2.928(2) Å
	O−H···N = 151.35(7)°	O−H···N = 152.84(7)°
nicotine−DITF	N···I (x − 1, y + 1, z + 1) = 2.869(4) Å	N···I = 3.02(3) Å
	N···I (x − 2, y, z) = 2.921(4) Å	N···I = 3.03(3) Å
nicotine−DOB	N···I = 2.808(5) Å	N···I = 2.91(5) Å
	I···N (2 − x, 1/2 + y, 1 − z) = 2.852(5) Å	I···N (1 − x, 1/2 + y,1 − z) = 2.97(6) Å
	N···I = 2.901(3) Å	N···I = 3.00(8) Å
	I···N (−x, 1/2 + y, 2 − z) = 2.934(5) Å	I···N (1 − x, 1/2 + y, 2 − z) = 2.91(5) Å

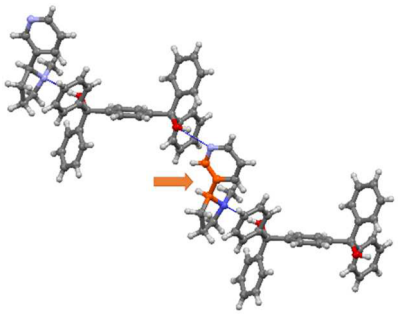

Figure 2. Crystal structure of nicotine-D1, showing the hydrogen bond pattern. Torsion angle τ (see text) is highlighted in orange.

involving the −OH groups of the D1 coformer as donors and both the nicotine nitrogen atoms as acceptors (Table 2), generating chains promoted by the anti orientation of the two nitrogen atoms (Figure 2).

Because of the wheel-and-axle shape of the coformer, the chains are assembled so that the D1 ligands are arranged in arrays of parallel molecules slightly offset to promote interdigitation of phenyl groups (Figure 3), as observed for families of similar organic and organometallic compounds.[32−34]

The role of the interactions between the coformer molecules in partially driving the packing is shown by the calculation of intermolecular potential energy performed by CrystalExplorer17 (Figure 3) and visualized by the energy framework method[35] (Figure 4). While the strongest interaction is between the hydrogen bonded molecules, the second major

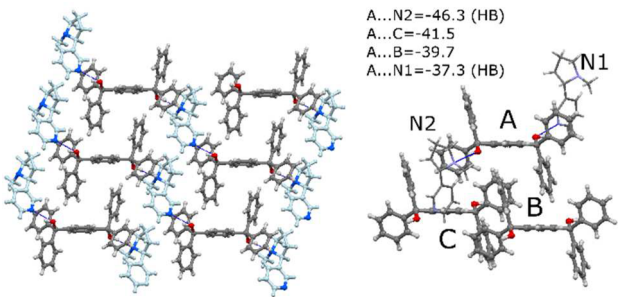

Figure 3. Left: arrays of hydrogen bonded chains in the crystal packing of nicotine−D1. Right: main interactions between neighboring molecules (kJ/mol), comprising hydrogen bonds (HB) and edge-to-face CH···π interactions between D1 molecules.

DOI: 10.1021/acs.cgd.7b00887
Cryst. Growth Des. XXXX, XXX, XXX−XXX

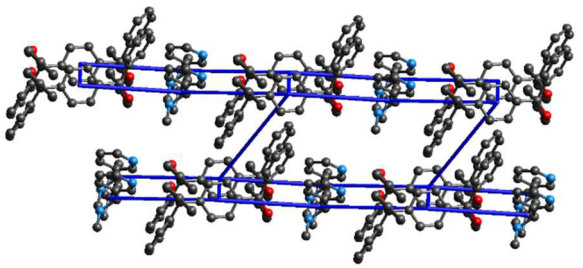

Figure 4. Energy framework for nicotine-D1, showing the four main interactions present in the packing.

source of packing stabilization is the offset stacking between D1 molecules. The MEP of D1, shown in Figure 1, justifies the offset stacking as a way to optimize edge-to-face interactions which bring into proximity the oppositely charged parts of the molecule.

Inspection of the packing energy framework (Figure 4) shows that the packing of the conformer D1 represent a scaffold to which nicotine adapts to optimize hydrogen bond interactions. The energy framework method consists in representing the interactions between nearest neighboring molecules as tubes connecting molecular centroids. Tubes diameter is proportional to the energy strength, so that the main interactions responsible of the crystal stabilization are visible at a glance.

Nicotine−DITF crystallizes in the $P2_1$ chiral space group, with a 1:1 stoichiometric ratio, and $Z' = 2$ (Figure 5). Both independent nicotine molecules present the anti conformation of the two rings, defined by torsion angles τ of 140° and 143°, respectively.

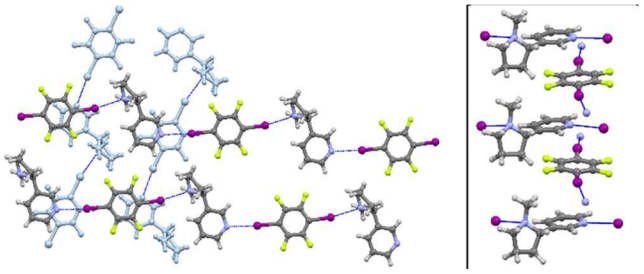

Figure 5. Crystal packing of nicotine−DITF, dominated by halogen bonded chains. Chains are tilted by 60°, as shown in shading. Inset: detail of close packing between tilted chains.

As expected from cocrystal design strategy, the packing topology is dominated by the halogen bonds between the iodinated coformer and the nicotine nitrogen atoms, featuring a chain motif topologically similar to the one observed with the D1 coformer (Table 2). However, in this case the halogen bonded chains are arranged in skew orientation, with an angle of 60° between the vectors describing adjacent chains, which are crystallographically independent. From the examination of the molecular electrostatic potential mapped on the molecular surface it is evident that the best fit between nicotine and DITF is reached with a parallel stacking of the pyridine on the tetrafluoro benzene ring, exploiting the complementary electrostatic potential of the two surfaces (Figure 1). Interaction of the negative fluorinated edge of DITF with the pyrrolidine positive surface is also stabilizing (Supporting Information). The halogen bonded chains are therefore tilted in order to optimize the fit between the pyrrolidine ring and DITF. Inspection of the energy framework (Figure 6) confirms that the main interaction dominating the packing is the stacking between nicotine and DITF, while the halogen bond adapts to this scaffold.

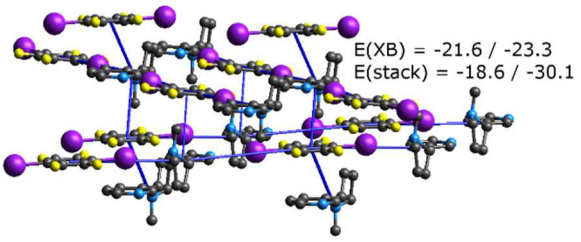

Figure 6. Energy framework representation for nicotine−DITF. Ranges of the energy of the halogen bonds (E(XB)) and stacking (E(stack))interactions relative to the pairs of independent molecules are reported in kJ/mol.

Nicotine−DOB crystallizes in the $P2_1$ chiral space group, with a 1:1 stoichiometry and $Z' = 4$ (Figure 7).

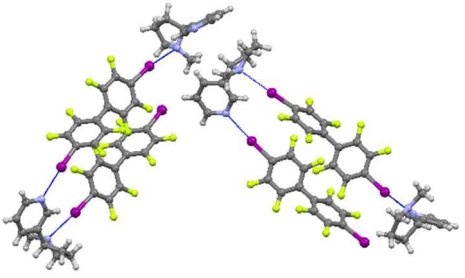

Figure 7. Four independent molecules in nicotine−DOB cocrystal. All the four nicotine molecules adopt the syn conformation to form halogen bonds, which are highlighted.

The four independent nicotine molecules present the same syn orientation of the nitrogen atoms on the two rings, defined by torsion angles τ respectively of −54°, −56°, −58°, and −59° around the single bond joining the rings. The crystal packing, as expected, is based on halogen bonds (Table 2) involving nicotine molecules which bridge arrays of stacked DOB molecules, in a ladder motif (Figure 8). In the crystal packing

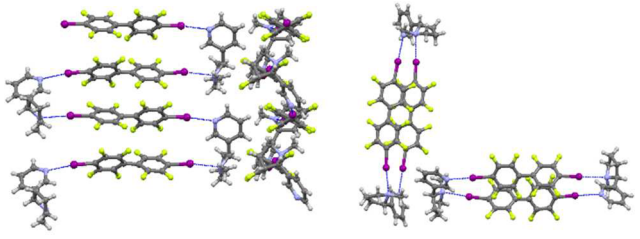

Figure 8. Left: two orthogonal ladder motifs are generated by halogen bonds with nicotine in the syn conformation. Right: edge-on view of the two independent ladders, tilted by 90°.

there are two independent arrays, tilted by about 90°. From the analysis of the molecular electrostatic potential (Figure 1) it is evident that, besides the halogen bonds, the stacking of DOB molecules is the stable motif driving the packing arrangement, because it allows the approach of the negative ridge of the

DOI: 10.1021/acs.cgd.7b00887
Cryst. Growth Des. XXXX, XXX, XXX−XXX

aromatic rings to the positively charged ring surface (Figure SI-7, Supporting Information).

The energy framework analysis (Figure 9) confirms that the predominant stabilization in the crystal packing is due to dispersive interactions between stacked DOB coformers.

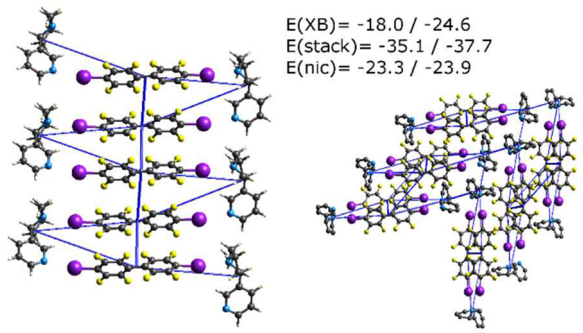

Figure 9. Energy framework representation for nicotine–DOB. Left: ladder motif; right: orthogonal arrangement of ladder motifs. Ranges of the energy of the interactions relative to the pairs of independent molecules are reported in kJ/mol. *E*(XB) refers to halogen bonds, *E*(stack) and *E*(nic) to DOB···DOB and nicotine···nicotine interactions, respectively.

Thermal Analysis. Differential scanning calorimetry (Figure 10) on nicotine–DITF (mp 109 °C) shows a neat

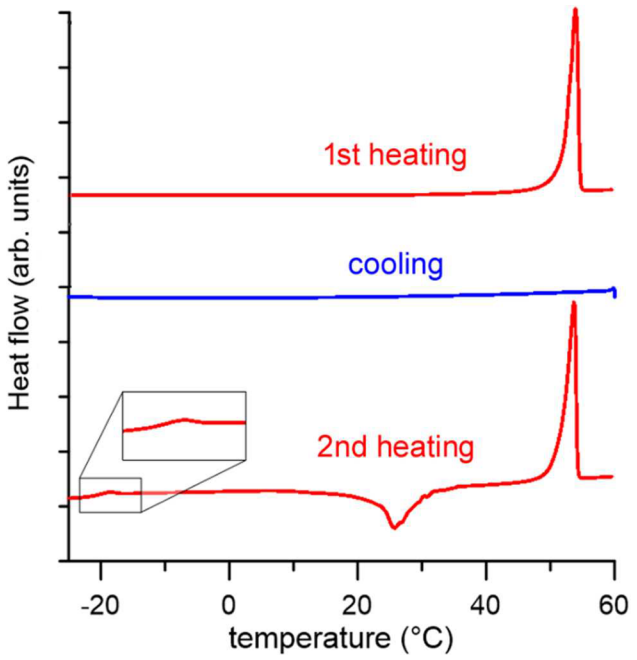

Figure 10. DSC experiment on nicotine–DITF cocrystal (endo up). Glass transition on the second heating ramp is magnified in the inset.

melting peak during the first heating run with a maximum at 54 °C (ΔH = 27.6 kJ/mol) (see also Supporting Information). During the cooling scan no phenomena are observed, while in the second heating run a glass transition appears between −22 °C and −18 °C. A broad exothermic peak, with a minimum at 26 °C (ΔH = −18.7 kJ/mol) represents the recrystallization of the cocrystal. The melting of the cocrystal is confirmed by the presence of a third peak in the DSC, endothermic, with a maximum at 54 °C (ΔH = 26.4 kJ/mol) and perfectly comparable, both for temperature and for enthalpy, to the melting peak of the first heating. This proves that the system is thermally reversible and degradation or loss of any components does not occur. The glass transition shows that the cocrystal is not ready to crystallize during the cooling phase, giving a glass. It is important to note that nicotine is characterized by glass transition which occurs below −79 °C; therefore, it is a definitely difficult molecule to crystallize, probably for the presence of multiple orientations of the two rings which generate free volume in the solid phase.

DSC analysis was performed on nicotine–DOB (mp 146 °C) (Supporting Information) following the typical first heating–cooling–second heating experiment. During the first heating an endothermic peak with a maximum at 68 °C (ΔH = 24.3 kJ/mol) is visible and ascribable to melting of the cocrystal. The cooling run is characterized by a progressive decrease in heat flow from 80 °C down to −20 °C, but no relevant peaks are present. During the second heating, a glass transition occurs between −10 °C and −5 °C, similarly to what has been observed for nicotine–DITF, but no recrystallization phenomena are observed.

DSC measurement on nicotine–D1 (mp 169 °C) points out a neat endothermic peak at 92 °C, related to the cocrystal melting (ΔH = 37.9 kJ/mol). During the cooling scan, no recrystallization phenomenon is detected. Similarly to nicotine–DOB and nicotine–DITF, a glass transition occurred also for nicotine–D1 during the second heating ramp, in the range between −27 to −15 °C. Like for nicotine–DOB, no recrystallization events are observed during the second heating scan. The melting point of all these cocrystals are intermediate between those of the pure components. Looking at the trend of the differences between the melting point of the cocrystals with respect to those of the coformers, it is seen that DITF has the smallest difference (55 °C), while DOB and D1 perform similarly (78 and 77 °C respectively).

DISCUSSION

From the thermal analyses it is evident that nicotine is awkward in achieving close-packing, given its tendency to form glass phases. This can be related to conformational frustration. Noticeably, nicotine was considered a rigid molecule, where the most stable conformation has the pyridine and pyrrolidine rings oriented roughly perpendicular to one another with the methyl and pyridyl substituents in the trans configuration with a torsional barrier of approximately 110 kJ/mol.[30] By contrast, a recent extensive computational exploration of nicotine gas-phase conformations has shown that the molecule presents eight lowest energy isomers in a range of 30 kJ/mol, and they were found to interconvert via low (<25 kJ/mol) rotational barriers around the pyridine–pyrrolidine bond.[36] The main variability described for these conformers refers to the puckering of the pyrrolidine ring, the reciprocal orientation of the methyl substituents and of the pyridine with respect to the pyrrolidine ring, and the rotation around the pyridine–pyrrolidine bond, indicated with τ in the previous discussion. In fact we observed two different major conformations in our structures, corresponding to the two lowest energy conformers found by the computational investigation, differing mainly for the reciprocal orientation of the two rings around the central bond, by approximately 2.5 kJ/mol[36] (for a comparison with the computations see Supporting Information). This means that the packing effects allow to sample different minima in the conformational landscape of nicotine. The conformational

DOI: 10.1021/acs.cgd.7b00887
Cryst. Growth Des. XXXX, XXX, XXX–XXX

variability of nicotine is reflected by the distribution of the torsion angle τ across the three crystal structures reported here (Figure 11), containing altogether seven conformers, combined with the two observed in the other cocrystal reported so far (CSD refcode KERSAB[13]), while the molecular structure of nicotine reported in ref 14 is too disordered to determine a reliable conformation.

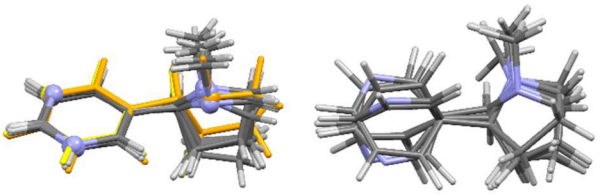

Figure 11. Left: comparison of the conformations observed in the crystal structures of nicotine cocrystals (KERSAB highlighted in yellow, nitrogen atoms evidenced to mark syn/anti geometries). Right: model conformational variability for nicotine based on analogue crystal structures form CSD conformer analysis.

In the two major conformations found here, one has torsion angle τ ranging from −54° to 59° (syn) and one has torsion angle τ ranging from 140° to 143° (anti). A screening of realistic conformations observed in the crystal structures of molecules similar to nicotine has been performed with the conformer generator module of the CSD system[37] and shows a remarkable variety of possible observable orientations of the two rings around the bond joining them (Figure 11, right). If on one hand this hampers a neat crystallization of the pure compound, it also makes nicotine adaptable to different packing environments, thus generating several possible packing motifs, depending on the reciprocal orientation of the two nitrogen atoms. Namely, one-dimensional chains are attained when nicotine occurs in anti conformation, while ladder motifs occur when nicotine displays a syn conformation. In the cocrystals reported here, the coformer···coformer interactions (wheel-and-axle arrangement in nicotine−D1, offset aromatic stacking in nicotine−DITF, DOB stacking in nicotine−DOB) govern the structural motifs found in the packing, while nicotine is ready to adapt its conformation in order to optimize the strong hydrogen bond, or halogen bond interactions formed through its nitrogen atoms. The strength of these interactions is shown by the fact that all the cocrystals reported here show melting temperature at least 130 °C higher than the melting temperature of −79 °C reported for pure nicotine.[38] Noticeably, form thermal data emerge that the hydrogen bonded coformer D1 could play a stronger stabilizing role, reflected in the higher melting enthalpy of the nicotine−D1 cocrystal.

CONCLUSIONS

"It's an odd case, Sir. Never come across a case of nicotine poisoning before in all my experience. No more has our Doctor Davis."

"I always thought it was a kind of disease you got from over-smoking."

"To tell the truth, so did I, Sir. But the doctor says that the pure alkaloid is an odorless liquid, and that a few drops of it are enough to kill a man almost instantaneously."

—*Three Act Tragedy*, Agatha Christie

Apart from its deadly aura related to the plague of tabagism[39] and to its high toxicity,[40] nicotine is an elusive molecule when we consider its ability to close pack in a crystalline form. Despite its molecular weight and complexity, nicotine is in fact a liquid with extremely low melting point, reluctant to crystallize. This can be related to its conformational frustration, and we have introduced the idea that this fact can be exploited to obtain cocrystals whose supramolecular arrangement is dictated by the coformer packing characteristics, and nicotine adapts to these. In this way we have obtained three new high melting forms of nicotine-containing compounds, which open the route to new methods of formulation of this ingredient in a solid form.

ASSOCIATED CONTENT

Supporting Information

The Supporting Information is available free of charge on the ACS Publications website at DOI: 10.1021/acs.cgd.7b00887.

Synthesis of D1 and DOB. ORTEP drawings of the crystal structures of nicotine−D1, nicotine−DITF, and nicotine−DOB. DSC plots for nicotine−DOB, nicotine−D1, and nicotine−DITF. Comparison of conformations in this work and from literature. MEP of nicotine and the coformers in the cocrystals (PDF)

Accession Codes

CCDC 1557603−1557605 contain the supplementary crystallographic data for this paper. These data can be obtained free of charge via www.ccdc.cam.ac.uk/data_request/cif, or by emailing data_request@ccdc.cam.ac.uk, or by contacting The Cambridge Crystallographic Data Centre, 12 Union Road, Cambridge CB2 1EZ, UK; fax: +44 1223 336033.

AUTHOR INFORMATION

Corresponding Author

*E-mail alessia.bacchi@unipr.it.

ORCID

Davide Balestri: 0000-0003-3493-9115

Paolo Pelagatti: 0000-0002-6926-2928

Alessia Bacchi: 0000-0001-5675-9372

Author Contributions

All authors have given approval to the final version of the manuscript.

Funding

D.C. was funded by a Regione Emilia-Romagna Spinner2013 grant. P.P.M. was funded by a grant from 'Bando per progetti di ricerca industriale strategica rivolti agli ambiti prioritari della Strategia di Specializzazione Intelligente (azione 1.2.2) Asse I POR FESR Emilia-Romagna 2014−2020'. D.B. was funded by CIRCC (Consorzio di Reattività Chimica e Catalisi).

Notes

The authors declare no competing financial interest.

ACKNOWLEDGMENTS

Nicola Demitri at the XRD1 beamline of Elettra Sincrotrone, Trieste is thanked for helpful assistance in data collection. The Laboratorio di Strutturistica Mario Nardelli at the University of Parma is acknowledged for in house data collection facilities.

REFERENCES

(1) Morissette, S. L.; Almarsson, O.; Peterson, M. L.; Remenar, J. F.; Read, M. J.; Lemmo, A. V.; Ellis, S.; Cima, M. J.; Gardner, C. R. *Adv. Drug Delivery Rev.* **2004**, *56* (3), 275−300.

DOI: 10.1021/acs.cgd.7b00887
Cryst. Growth Des. XXXX, XXX, XXX−XXX

(2) Metcalf, R. L.; Horowitz, A. R. *Ullmann's Encyclopedia of Industrial Chemistry*; Wiley: New York, 2014; pp 123
(3) Ujváry, I. In *Nicotinoid Insecticides and the Nicotinic Acetylcholine Receptor*; Springer, 1999; pp 29−69.
(4) Graton, J.; Van Mourik, T.; Price, S. L. *J. Am. Chem. Soc.* **2003**, *125* (19), 5988−5997.
(5) Duggirala, N. K.; Perry, M. L.; Almarsson, Ö.; Zaworotko, M. J. *Chem. Commun.* **2016**, *52*, 640−655.
(6) Bacchi, A.; Capucci, D.; Giannetto, M.; Mattarozzi, M.; Pelagatti, P.; Rodriguez-Hornedo, N.; Rubini, K.; Sala, A. *Cryst. Growth Des.* **2016**, *16* (11), 6547−6555.
(7) McKellar, S. C.; Kennedy, A. R.; McCloy, N. C.; McBride, E.; Florence, A. J. *Cryst. Growth Des.* **2014**, *14* (5), 2422−2430.
(8) Luo, Y.-H.; Zhang, C.-G.; Xu, B.; Sun, B.-W. *CrystEngComm* **2012**, *14* (20), 6860.
(9) Lemmerer, A.; Fernandes, M. a. *New J. Chem.* **2012**, *36* (11), 2242.
(10) Kirchner, M. T.; Bläser, D.; Boese, R. *Chem. - Eur. J.* **2010**, *16* (7), 2131−2146.
(11) Aakeröy, C. B.; Wijethunga, T. K.; Benton, J.; Desper, J. *Chem. Commun.* **2015**, *51* (12), 2425−2428.
(12) Aakeröy, C. B.; Wijethunga, T. K.; Desper, J. *Chem. - Eur. J.* **2015**, *21* (31), 11029−11037.
(13) Fukawa, K.; Harada, S.; Kasai, N.; Toda, M.; Mori, K.; Toda, F. *Bull. Chem. Soc. Jpn.* **1989**, *62* (8), 2714−2716.
(14) Sanna, E.; Escudero-Adán, E. C.; Bauzá, A.; Ballester, P.; Frontera, A.; Rotger, C.; Costa, A. *Chem. Sci.* **2016**, *7*, 2439.
(15) Kaminski, K.; Paluch, M.; Ziolo, J.; Ngai, K. L. *J. Phys.: Condens. Matter* **2006**, *18*, 5607−5615.
(16) Aakeröy, C. B.; Wijethunga, T. K.; Haj, M. A.; Desper, J.; Moore, C. *CrystEngComm* **2014**, *16* (31), 7218.
(17) Espallargas, G. M.; Recuenco, A.; Romero, F. M.; Brammer, L.; Libri, S. *CrystEngComm* **2012**, *14* (20), 6381.
(18) Plietzsch, O.; Schade, A.; Hafner, A.; Huuskonen, J.; Rissanen, K.; Nieger, M.; Muller, T.; Bräse, S. *Eur. J. Org. Chem.* **2013**, *2013* (2), 283−299.
(19) Kabsch, W. *Acta Crystallogr., Sect. D: Biol. Crystallogr.* **2010**, *66* (2), 125−132.
(20) Sheldrick, G. M. *Acta Crystallogr., Sect. A: Found. Crystallogr.* **2008**, *64* (1), 112−122.
(21) Dolomanov, O. V.; Bourhis, L. J.; Gildea, R. J.; Howard, J. A. K.; Puschmann, H. *J. Appl. Crystallogr.* **2009**, *42* (2), 339−341.
(22) Groom, C. R.; Bruno, I. J.; Lightfoot, M. P.; Ward, S. C. *Acta Crystallogr., Sect. B: Struct. Sci., Cryst. Eng. Mater.* **2016**, *72* (2), 171−179.
(23) Turner, M. J.; McKinnon, J. J.; Wolff, S. K.; Grimwood, D. J.; Spackman, P. R.; DJ, S, M. A. University of Western Australia, 2017.
(24) Turner, M. J.; Grabowsky, S.; Jayatilaka, D.; Spackman, M. A. *J. Phys. Chem. Lett.* **2014**, *5* (24), 4249−4255.
(25) Jayatilaka, D.; Grimwood, D. J. *Comput. Sci. - Iccs 2003, Pt Iv, Proc.* **2003**, *2660*, 142−151.
(26) Hunter, C. A. *Angew. Chem., Int. Ed.* **2004**, *43* (40), 5310−5324.
(27) Gavezzotti, A. *CrystEngComm* **2003**, *5* (77), 439−446.
(28) Aakeröy, C. B.; Wijethunga, T. K.; Desper, J. *New J. Chem.* **2015**, *39* (2), 822−828.
(29) Perera, M. D.; Desper, J.; Sinha, A. S.; Aakeröy, C. B. *CrystEngComm* **2016**, *18* (44), 8631−8636.
(30) Graton, J.; Berthelot, M.; Gal, J. F.; Girard, S.; Laurence, C.; Lebreton, J.; Le Questel, J. Y.; Maria, P. C.; Naus, P. *J. Am. Chem. Soc.* **2002**, *124* (35), 10552−10562.
(31) Aakeroy, C. B.; Wijethunga, T. K.; Desper, J.; Dakovic, M. *Cryst. Growth Des.* **2016**, *16* (5), 2662−2670.
(32) Bacchi, A.; Carcelli, M. *Structure and Function* **2010**, 235−253.
(33) Bacchi, A. In *Models, Mysteries and Magic of Molecules*; Springer, 2008; pp 87−108.
(34) Bacchi, A.; Carcelli, M.; Pelagatti, P. *Crystallogr. Rev.* **2012**, *18* (4), 253−279.
(35) Turner, M. J.; Thomas, S. P.; Shi, M. W.; Jayatilaka, D.; Spackman, M. A. *Chem. Commun.* **2015**, *51* (18), 3735−3738.
(36) Yoshida, T.; Farone, W. A.; Xantheas, S. S. *J. Phys. Chem. B* **2014**, *118* (28), 8273−8285.
(37) Taylor, R.; Cole, J.; Korb, O.; McCabe, P. *J. Chem. Inf. Model.* **2014**, *54* (9), 2500−2514.
(38) Lide, D. R. *CRC Handbook of Chemistry and Physics*, 88th ed.; CRC Press, Taylor&Francis, 2007.
(39) Kluger, R. *Ashes to Ashes*; Knopf, 1998.
(40) Arneric, S. P., Brioni, J. D. *Neuronal Nicotinic Receptors: Pharmacology and Therapeutic Opportunities*; Wiley: New York, 1998.

DOI: 10.1021/acs.cgd.7b00887
Cryst. Growth Des. XXXX, XXX, XXX−XXX